Journal of
Applied Remote Sensing

Accurate detection of tree apexes in coniferous canopies from airborne scanning light detection and ranging images based on crown-extraction filtering

Fumiki Hosoi
Hiroaki Matsugami
Kenichi Watanuki
Yo Shimizu
Kenji Omasa

Accurate detection of tree apexes in coniferous canopies from airborne scanning light detection and ranging images based on crown-extraction filtering

Fumiki Hosoi, Hiroaki Matsugami, Kenichi Watanuki, Yo Shimizu, and Kenji Omasa
The University of Tokyo, Graduate School of Agricultural and Life Sciences, Bunkyo-ku, Tokyo 113-8657, Japan
E-mail: aomasa@mail.ecc.u-tokyo.ac.jp

Abstract. We describe crown-extraction (CE) filtering to accurately determine tree apex positions for various coniferous species using an airborne light detection and ranging–derived digital canopy height model (DCHM). This method uses a square mask, with a frame at the edges, that overlaps pixels within the DCHM image; when no pixels touch the frame, the pixel at the center is extracted as a tree-crown pixel. The apex of each tree is determined by choosing the pixel with maximum height from the pixels in the crown. We compared the performance of this method and of two other methods (local-maximum filtering and canopy-segmentation method) for several species. The CE filtering had the most accurate results for most tree species with appropriate mask size selection. The mean omission, commission, and total errors for all tree species were 8.1%, 1.6%, and 9.7%, respectively, for CE filtering. Comparing mask sizes and canopy diameters estimated from the DCHM for each species revealed that the smallest canopy diameter of each species was close to the most appropriate mask size for that species in CE filtering. We also confirmed that the smoothing process used in the DCHM has little effect on the accuracy of CE filtering. © *2012 Society of Photo-Optical Instrumentation Engineers (SPIE).* [DOI: 10.1117/1.JRS.6.063502]

Keywords: airborne scanning light detection and ranging; coniferous tree; digital canopy height model; tree apex.

Paper 10140 received Sep. 14, 2010; revised manuscript received Nov. 30, 2011; accepted for publication Dec. 28, 2011; published online Mar. 12, 2012.

1 Introduction

Light detection and ranging (LIDAR), an active remote-sensing technique that uses a laser scanner, has been used to measure canopy structure. Mapping of tree apexes in a LIDAR image is very important because spatial distribution of tree heights can be obtained from the map, so that the distribution is associated with spatial heterogeneity of biophysical properties of trees, such as aboveground biomass or carbon stocks using allometric relationships between these properties and the tree heights.[1–5] Information of such spatial heterogeneity would be useful for understanding of plant functions such as photosynthesis and transpiration and determining suitability of different habitats for various species. Thus, a method for accurate mapping of tree apexes in a LIDAR image is needed.

The use of airplane-mounted scanning LIDAR for canopy measurements started in the mid-1990s.[6,7] Airborne LIDAR with a large footprint and a large scan width was developed for remote sensing of forests at large scales.[8–12] However, the image resolution is too coarse to allow for determination of the canopy structure at the scale of individual trees. On the other hand, commercially available small-footprint airborne LIDAR systems have been widely used to measure canopy structure.[1–5,13–25] In the 1990s, the density of laser pulses provided by ordinary small-footprint airborne scanning LIDAR systems was about 1 pulse per m^2 on the ground at flying altitude of 500 to 1000 m, with a pulse repetition frequency of 1 to 33 kHz. The resolution

0091-3286/2012/$25.00 © 2012 SPIE

of these systems was not sufficiently fine to produce a precise 3-D image at the scale of individual trees. Recent advances in LIDAR technology have increased the scanning density to >10 pulse per m^2, with a pulse repetition frequency of >200 kHz. Moreover, the density can be increased several-fold by using helicopters, which permit slower flight speeds than fixed-wing aircraft, as the platform.[1,13,14] A high-resolution image obtained from a LIDAR system with a high pulse density can provide images of sufficient resolution to allow measurement of the structural characteristics of individual trees.[1,2,13–21] To extract tree heights from LIDAR images, it is necessary to accurately detect the position of each tree's apex. Several methods can be used to calculate the positions of tree apexes for coniferous species.[18,19,21–27] Local-maximum (LM) filtering was originally developed to detect tree apexes in aerial photographs,[26,27] but can also be applied to LIDAR images.[23,24] In this method, local maxima within the image are identified using a search window whose size changes based on the semivariance range or slope break calculated for each of pixels and on the relationships between tree height and crown size derived from field inventory data.[23] The local maxima are then regarded as tree apexes. Actually, the method is difficult to use when the goal is to provide accurate results for a range of coniferous tree species with different canopy structures, as shown in a previous study.[24] An alternative, the canopy-segmentation method, is based on the watershed algorithm, and has become a popular method to delineate canopy boundaries.[18,19,21,25] In this method, pixels corresponding to local maxima are identified in a smoothed LIDAR image by searching for pixels whose height values are greater than those of any of the eight neighboring pixels. These pixels are regarded as tree apexes. Computation using this method is easier than in LM filtering because the search window size is fixed at 3×3 pixels. However, the accuracy is sensitive to the strength of the smoothing,[25] and it is often difficult to determine the most appropriate strength for stands that contain a variety of canopy structures. Thus, it is also difficult to obtain accurate results with this method for a range of coniferous species with different canopy structures.

Thus, there is still a lack of techniques for detecting tree apexes in heterogeneous multispecies canopies from airborne LIDAR images. In the present paper, we propose an alternative form of crown-extraction (CE) filtering, which we developed to accurately identify tree apexes of various coniferous species from airborne LIDAR images. We tested the method for several coniferous species and compared its accuracy with that of the LM and canopy-segmentation (CS) methods.

2 Materials and Methods

2.1 *Study Sites*

We chose two study sites for the experiments. Site 1 was a forest with nearly flat topography located near Tazawa Lake, Akita Prefecture, Japan (39°37′N, 140°38′E[1]). Japanese cedar (*Cryptomeria japonica*) trees dominated the forest. The trees were about 50 years old. At this site, we identified a region [Fig. 1(a), broken lines] containing 62 cedar trees. Site 2 was an urban park, the Shinjuku Gyoen National Garden, in central Tokyo (35°41′N, 139°42′E).[14] About 250 species and 2000 trees grow there. Two regions within site 2 [Figs. 1(b) and 1(c); broken lines] included 42 deodar cedars (*Cedrus deodara*), 17 Lebanon cedars (*Cedrus libani*), 14 Japanese black pines (*Pinus thunbergii*), and 11 dawn redwoods (*Metasequoia glyptostroboides*).

2.2 *Helicopter-Borne Scanning LIDAR Measurements*

Sites 1 and 2 were scanned in May 1998 and November 2001, respectively, using a helicopter-borne scanning LIDAR system (ALTM 1025 special model; Optech Co. and Aero Asahi Co.; Table 1).[1,14] The LIDAR system calculated the distance to a target by measuring the elapsed time between the emitted and returned laser pulses (the time-of-flight method). The laser wavelength was 1064 nm and the range accuracy was ± 15 cm, with a resolution of 1 cm. The system had two receiving modes—the first-pulse (FP) and last-pulse (LP) modes—in which the first and last returned laser pulses, respectively, were detected. Laser pulses illuminating the canopy surface

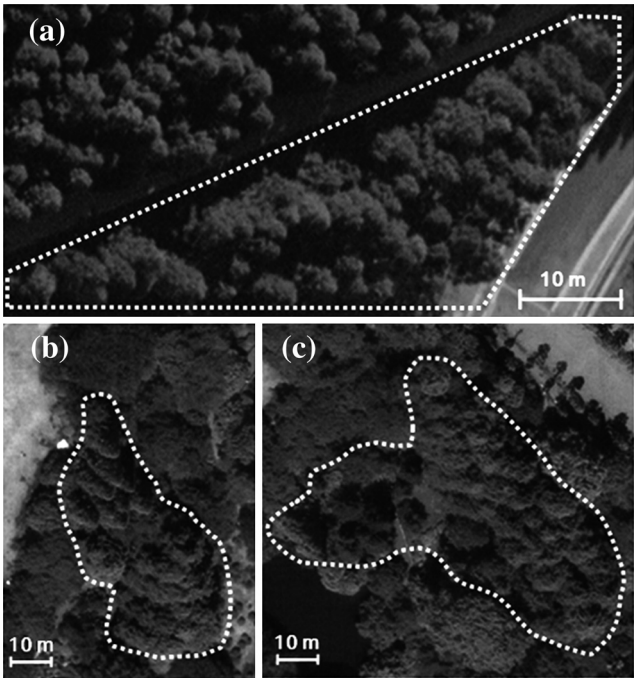

Fig. 1 Aerial photographs of the two study sites. The regions surrounded by broken lines are the measurement plots. (a) Site 1, located near Tazawa Lake, Akita Prefecture, Japan. (b) and (c) Site 2, located in the Shinjuku Gyoen National Garden in central Tokyo, Japan.

Table 1 Specifications of the helicopter-borne scanning LIDAR system.[1,14]

	Site 1	Site 2
Type	ALTM 1025 special model	ALTM 1025 special model
Flight height (m)	160 to 200	300
Flight speed ($km\,h^{-1}$)	50	60
Laser wavelength (nm)	1064	1064
Range accuracy (cm)	15	15
Range resolution (cm)	1	1
Repetition frequency (kHz)	25	25
Scanning frequency (Hz)	25	20
Scanning angle (degree)	11.3	10.0
Receiving modes	First and last pulse modes	First and last pulse modes
Beam divergence (mrad)	1.2	1.0
Footprint size (cm)	20–30	30
Footprint interval (cm)	Flight direction: 10–15 Scan direction: 28	Flight direction: 17 Scan direction: 42

were received as FP-mode data, and pulses that reached the ground surface were received as LP-mode data. During measurements, the flight speed and flight height were 50 $km\,h^{-1}$ and 160 to 200 m, respectively, at site 1 and 60 $km\,h^{-1}$ and about 300 m at site 2.

The repetition frequency and scanning frequency were 25 kHz and 25 Hz, respectively, at site 1 and 25 kHz and 20 Hz at site 2. The maximum scanning angle off-nadir and the beam divergence were 11.3 deg and 1.2 Mrad, respectively, at site 1 and 10.0 deg and 1.0 Mrad at site 2. The footprint sizes on the ground were 20 to 30 cm at site 1 and about 30 cm at site 2. The footprint intervals (i.e., the distance between the centers of adjacent laser beams on the ground) were 10 to 15 cm in the flight direction and 28 cm in the scan direction at site 1, versus about 17 cm and about 42 cm, respectively, at site 2. By comparing the diameters and intervals of the footprints on the ground, we confirmed that the laser pulses covered most of the woody canopy surface. The geographic position of the data was determined with a helicopter-borne inertial measurement unit (IMU) and high-resolution global positioning system (GPS) receivers both in the helicopter

and on the ground. The point coordinates of both the FP-mode and LP-mode data were determined from the GPS data recorded in the helicopter and on the ground.

2.3 *Generation of Canopy and Site Models from the LIDAR Data and Ground Measurements*

We reconstructed the canopy surfaces at both sites as digital elevation models (DEMs) generated from the FP-mode data. We reconstructed the ground surfaces as digital terrain models (DTMs) by interpolating ground-level points extracted from the LP-mode data. To extract ground level points, LP-mode data was divided by square meshes with a certain size and lowest points within each mesh were selected as candidates of ground points. Then, slopes between each of the candidates and the neighboring ones were calculated and the ground points were selected based on the threshold value of the slope. We generated digital canopy-height models (DCHMs), which express the net canopy height after accounting for undulation of the ground surface, by subtracting the DTM elevations from the FP-mode DEM elevations at each site.[1,14] These models had a mesh size of 10×10 cm at site 1 and 33×33 cm at site 2, and were produced using a software made by TopScan, ERDAS IMAGINE (Leica Geosystems GIS & Mapping). The correct positions of the tree apexes in the generated DCHMs were determined using ground measurements in December 1998 for site 1 and December 2005 for site 2.

Before performing the ground measurements, we estimated the positions of the tree apexes from the DCHMs by manually identifying the local maxima and creating a position map for the tree apexes. The resulting map included both the true tree apexes and local maxima at different locations from the tree apexes. These local maxima represented unevenness in the canopy surface. We then identified the true positions of the tree apexes on the ground by measuring the distance between stems using a tape measure; this step allowed us to remove the local maxima different from tree apexes from the map. The accuracy of tree apex positions on the map based on the ground measurement was estimated to between 10 and 40 cm. Together with the tree apex identification, we also identified the species of each tree on the ground and recorded it on the map. We used this map subsequently for validation of the accuracy of the tree apex detection methods.

2.4 *Determination of Tree Apexes*

Figure 2 shows the sequence we followed for determination of the tree apexes by means of CE filtering. During the pretreatment process, we first removed the spike noise included in the original DCHM image at each site using a median filter with a mask size of 3×3 pixels, followed by smoothing of the image using a Gaussian filter. We then applied CE filtering to the images to extract the tree crowns. We defined a tree crown as the top portion of a tree's canopy that included an apex. The extracted tree crowns overlapped in the non-smoothed DCHM image, and the pixel with the highest value in each tree crown was identified as the tree apex.

In CE filtering, a distinctive feature of a conifer's canopy shape is utilized to extract each tree crown. When a coniferous canopy is cut by a horizontal plane at certain height and projected onto the horizontal plane, the projection forms a roughly circular or elliptical region (i.e., a region defined by a certain radius, or by a semi-major and semi-minor radius, from the center).

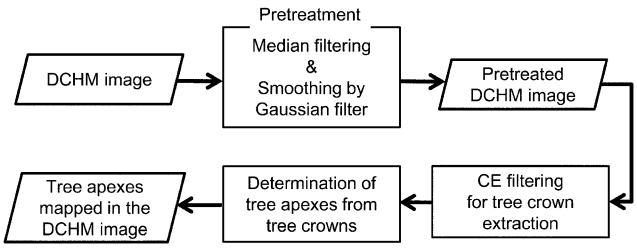

Fig. 2 The sequence followed to determine tree apex position by means of CE filtering.

A tree crown can therefore be projected around the center. In the DCHM image, the projection is equivalent to the pixels whose height values are equal to or higher than a certain height; in Fig. 3 (parts I and II), this height is expressed as a-a' to d-d'. It is possible to prepare a mask whose pixel values are 1 at the center and edges and 0 at other points (Fig. 3, part VI); that is, the edges of the mask form a square frame. The mask can be overlapped on a certain part of the projection, and if the border of the projection does not touch the frame of the mask, the mask's center is considered to be located around the center of the projection, and a pixel corresponding to the mask center is identified as part of the tree's crown [parts (b) to (d) in Fig. 3, parts III and IV].

The actual determination process is as follows: First, pixel values in the DCHM image are multiplied by the values of the mask at positions corresponding to those pixels. When the multiplication simultaneously yields non-zero values at the center of the mask and zero values at the edges, the pixel corresponding to the center of the mask is considered to be one of the pixels that compose the tree's crown. This process starts at lower heights and is repeated at progressively greater heights, step by step, using a height interval of 10 cm [Fig. 3(a) to 3(d), in sequence]. Moving from Fig. 3(a) to 3(d), zero, one, five, and one pixels, respectively, are identified as the pixels that comprise the tree's crown. Next, the logical disjunction of the pixels is calculated and the pixels that compose a tree's crown are determined based on the results of this calculation (Fig. 3, step V). Next, the mask is moved horizontally by one pixel within the DCHM image and these processes are repeated for all pixels within the DCHM image, so that each set of pixels that compose a single tree crown is determined. Each tree apex is then derived as the highest point in the identified crowns.

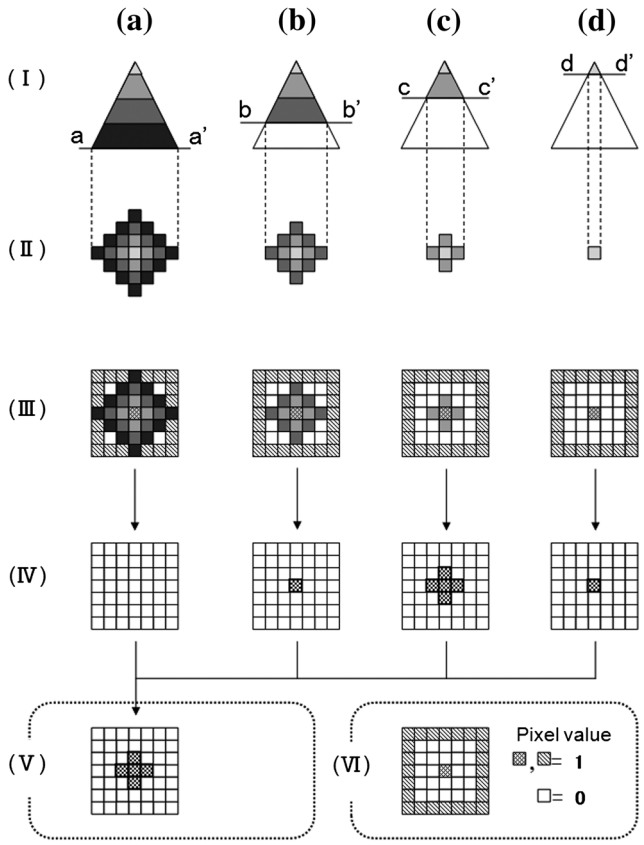

Fig. 3 Illustration of the process used in CE filtering. (a) to (d) represent different heights within the canopy, and represent different cross-sections of the canopy (a-a', b-b', c-c', and d-d', respectively). (I) Side views of the canopy in a DCHM. (II) Selected pixels at each height level. (III) The mask used in the CE filtering is overlapped on the selected pixels at each height level. (IV) The result of this overlapping is the group of pixels at a given height that belong to the tree's crown. (V) A logical disjunction is calculated for the pixels identified in (IV). (VI) An example of a typical mask used in CE filtering.

In this paper, we used square masks of dimensions $L \times L$, where L is measured in meters. For example, in Fig. 3, the masks are 7×7 squares, so a pixel size of 0.1 m would mean that $L = 0.7$ m. At the beginning of our analysis, we did not know the most appropriate mask size to use in the CE filtering. To determine this size, we performed CE filtering with mask sizes ranging from $L = 0.7$ to 2.9 m, with a pixel size of 0.1 m $\times$ 0.1 m, using a DCHM image of site 1 after smoothing using a weak Gaussian filter, with a standard deviation (σ) of $1/\pi$ and a radius of 1 pixel (= the integer that is closest to the value of 2σ). We estimated the errors in the detected apexes by comparing the detected apex positions with the positions in the field survey map described in Sec. 2.3. We determined the most appropriate mask size by comparing the errors in tree apex detection among all mask sizes.

Because the effect of smoothing of the DCHM image on the accuracy of tree apex detection was also unknown, we first applied CE filtering with the most appropriate mask size to the nonsmoothed DCHM image of site 1 (i.e., the image after only applying the median filter). We compared this result with the results of smoothing using Gaussian filters of different strength (i.e., with $\sigma = 1/\pi, 4/\pi, 6/\pi$, and $8/\pi$ and with the radius of the integer that is closest to the value of 2σ). The strength of the Gaussian filter increases as σ increases. We investigated the effect of this smoothing by comparing the errors of tree apex detection among the images created using different levels of smoothing. Tree apex positions were also detected for the DCHMs for site 2 by means of CE filtering. As was done for site 1, we determined the most appropriate mask sizes for site 2 for each tree species by evaluating the accuracy of apex detection using different mask sizes. We selected the strength of the Gaussian filters for site 2 based on the results for site 1.

We also used the nonsmoothed and smoothed DCHM images of site 1 for tree apex detection by means of LM filtering.[26] In this method, the windows were overlain on a DCHM image and a pixel corresponding to the center of the window was regarded as the local-maximum point and therefore as a tree apex if the pixel had the highest value of all pixels within the window. We varied the window size based on the semivariance range in each of the pixels (see Ref. 26 for more details about the calculation). We applied this method to site 1 using different strengths of Gaussian filter (i.e., with $\sigma = 1/\pi$, $4/\pi$, $6/\pi$, and $8/\pi$ and with the radius of the integer that is closest to the value of 2σ), and investigated the effect of smoothing by comparing the errors of tree apex detection among images with different levels of smoothing. We also performed tree apex detection in the DCHMs for site 2 using Gaussian filters whose strength was determined based on the results for site 1.

In the CS method,[18] pixels corresponding to local maxima were identified from a smoothed LIDAR image by searching for pixels whose height values were greater than those of the eight neighboring pixels. These local maxima were regarded as tree apexes. We applied this method to site 1, after changing the strength of the Gaussian filters used in the smoothing (i.e., with $\sigma = 1/\pi$, $4/\pi$, $6/\pi$, and $8/\pi$ and with the radius of the integer that is closest to the value of 2σ), and compared the errors among the results obtained using different filter strengths. We also applied this method to the DCHMs for site 2 using the filter strength determined based on the results for site 1.

Based on the tree apex detection results for sites 1 and 2, we compared the performance of the three methods for each tree species in the sample images. To provide a guideline for determining the most appropriate mask size to use in CE filtering, we investigated the relationship between the most appropriate mask size and the canopy diameter (i.e., the diameter of the canopy's vertical projection onto the ground, which was estimated manually using the DCHM images) for each species.

3 Results

Figure 4 shows the images of site 1 resulting from tree apex detection by means of CE filtering. Figure 4(a) shows a DCHM image of site 1 after the median filtering and smoothing using a Gaussian filter with $\sigma = 1/\pi$. This process removed the spike noise from the image, although some line noise remained at the right edge of the image. Figure 4(b) represents the tree crowns extracted by means of CE filtering with a mask size of $L = 1.9$ m. Note that each tree crown included several pixels and that the crowns were distributed almost evenly throughout the image.

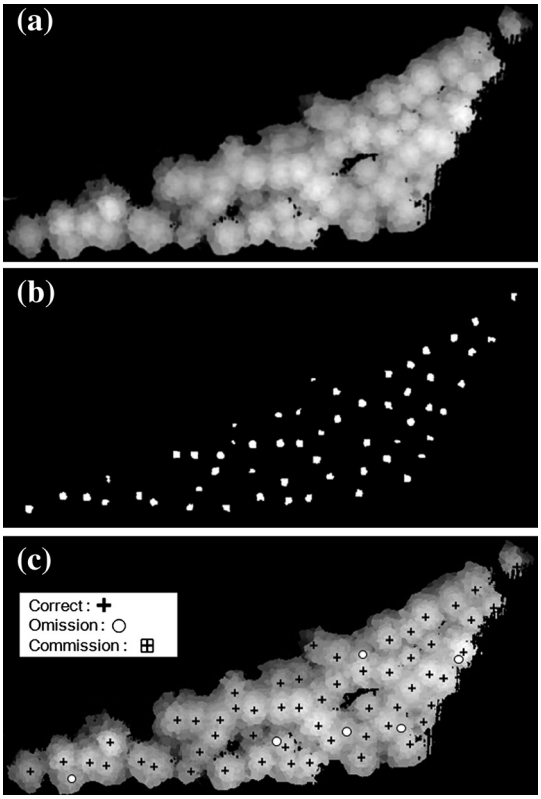

Fig. 4 Canopy images of site 1 resulting from the tree apex detection process by means of CE filtering. (a) A DCHM image of site 1 after the median filtering and smoothing using a Gaussian filter with $\sigma = 1/\pi$. (b) Tree crowns extracted by means of CE filtering with a mask size of $L = 1.9$ m. and (c) The result of tree apex detection mapped on the nonsmoothed DCHM image.

Figure 4(c) shows the results of the tree apex detection. Here and in the other methods of apex detection, there were two types of error of tree apex detection: omission errors, in which a tree apex was not detected, and commission errors, in which a pixel was incorrectly classified as a tree apex. The CE filtering detected most tree apexes correctly, and we observed no commission errors in the results. The total error in tree apex detection was 9.7%.

Figure 5 shows the results of CE filtering of the DCHM image shown in Fig. 4(a) using mask sizes ranging from $L = 0.7$ to 2.9 m. The number of commission errors increased drastically as mask size decreased below $L = 1.7$ m, whereas the number of omission errors increased slightly as the mask size increased beyond $L = 2.1$ m. Consequently, the minimum total number of errors occurred at a mask size of $L = 1.9$ m, which we therefore chose as the most appropriate mask size for the DCHM for site 1.

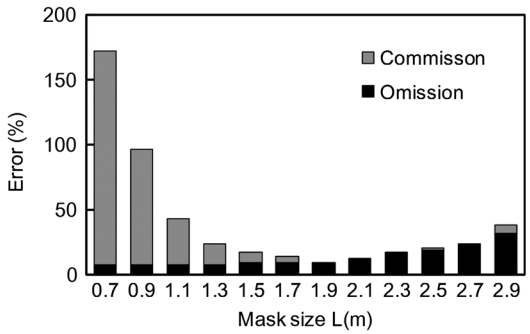

Fig. 5 Errors in tree apex detection at site 1 using CE filtering at various mask sizes $L(m)$.

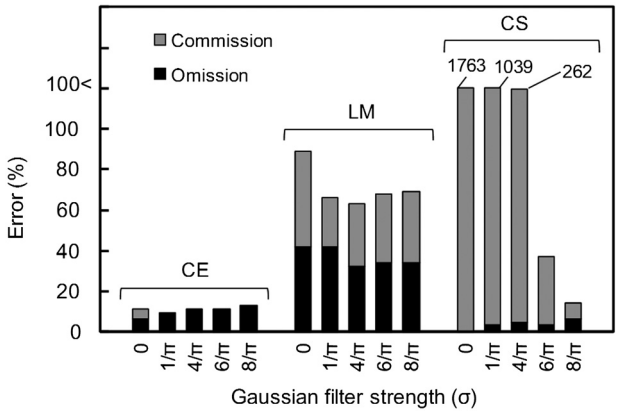

Fig. 6 Errors of tree apex detection using the DCHM image of site 1 as a function of the strength of the Gaussian filtering (standard deviation, σ) for the three detection methods. CE: crown-extraction filtering; LM: local-maximum method; CS: canopy-segmentation method.

Figure 6 summarizes the errors in tree apex detection using the DCHM image of site 1 for each strength of Gaussian filtering in the three detection methods. In the LM method, the omission error was lowest at $\sigma = 4/\pi$ but remained similar as σ increased beyond this point, whereas the commission error was lowest at $\sigma = 1/\pi$ and gradually increased at higher values. Consequently, the total error was lowest (63.0%) at $\sigma = 4/\pi$. Although smoothing by the Gaussian filter reduced the error in the LM method, large errors (greater than 60%) were found at all strengths of the Gaussian filter. In the CS method, the commission errors were extremely large at $\sigma = 4/\pi$ or lower, and decreased drastically as the strength of the Gaussian filter increased, whereas omission errors were small at all strengths of the Gaussian filter. Consequently, the total error was dominated by the commission error, and reached its minimum value (14.5%) at the strongest Gaussian filter we tested ($\sigma = 8/\pi$). These results demonstrate that this method was highly sensitive to the strength of the Gaussian filter. In the CE filtering, commission errors decreased to zero at $\sigma = 1/\pi$ or greater, and omission errors slightly increased as the strength of the Gaussian filter increased; thus, the total error was only slightly affected by the smoothing strength, and remained small at all filter strengths that we tested. The minimum total error was 9.7% at $\sigma = 1/\pi$.

Figure 7 shows the best tree apex detection results using the LM and CS methods, mapped using the non-smoothed DCHM of site 1. In the LM method, omission errors were frequent and

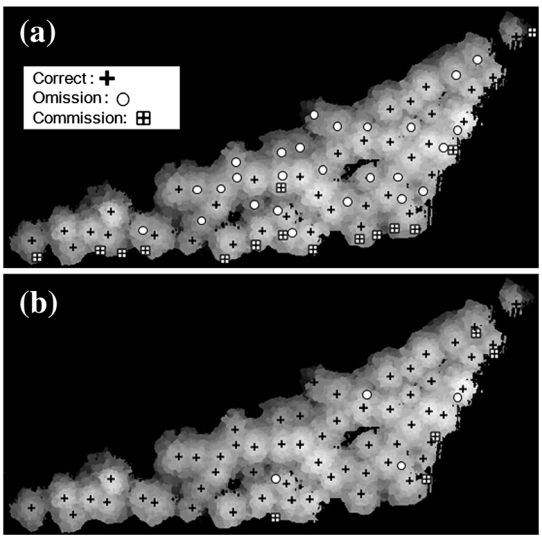

Fig. 7 Errors of tree apex detection using (a) the local-maximum method and (b) the canopy-segmentation method, mapped using the non-smoothed DCHM for site 1.

were distributed almost evenly throughout the image, whereas most commission errors were distributed along the lower and right edges of the image. In the CS method, most commission errors also occurred along the edges of the map, although there were fewer total errors than in the LM method. The omission, commission, and total errors in the best results for site 1 were 32.0%, 31.0%, and 63.0%, respectively, for the LM method and 6.0%, 8.0%, and 14.0% for the CS method.

Figure 8 shows the tree apex detection results for site 2 using the three detection methods, mapped using the nonsmoothed DCHMs for the site. Although many errors were observed in the LM method, fewer errors were observed in the other methods. In particular, most tree apexes were detected correctly by the CE filtering, so this method was the most accurate method overall. The mean omission, commission, and total errors at site 2 were 7.7%, 2.1%, and 9.8%, respectively, for the CE filtering, versus 46.3%, 9.0%, and 55.3% for the LM method and 12.0%, 6.5%, and 18.5% for the CS method.

Figure 9 summarizes the tree apex detection errors in the three methods for all species at sites 1 and 2. In the CE filtering, there were relatively few errors (an error of less than 20%) for all tree species. The method performed particularly well for dawn redwoods, for which we observed no errors. We observed more omission errors than commission errors for all species in this method.

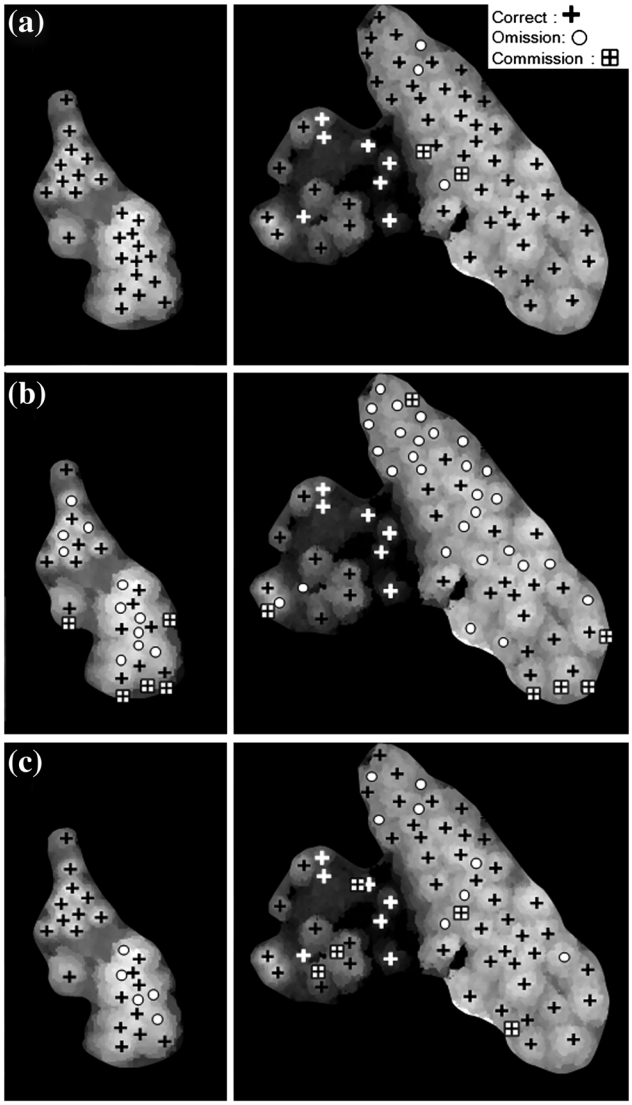

Fig. 8 Errors of tree apex detection using (a) crown-extraction (CE) filtering, (b) the local-maximum method, and (c) the canopy-segmentation method, mapped using the non-smoothed DCHMs for site 2.

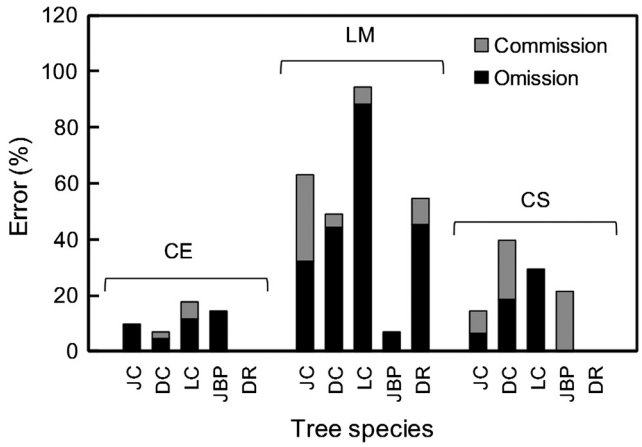

Fig. 9 Errors of tree apex detection using CE filtering, the local-maximum (LM) method, and the CS method for all tree species at sites 1 and 2. JC: Japanese cedar; DC: deodar cedar; LC: Lebanon cedar; JBP: Japanese black pine; DR: dawn redwood.

The most appropriate mask sizes in the CE filtering were $L = 1.9$ m for Japanese cedar, 4.3 m for Deodar cedar, 3.6 m for Lebanon cedar, and 4.3 m for Japanese black pine. By comparing these mask sizes with the canopy diameters estimated from the DCHMs, we confirmed that the most appropriate mask sizes were nearly equal to the smallest canopy diameter of each species estimated from the DCHM (i.e., 1.9, 4.3, 3.4, and 4.0 m, respectively). For the dawn redwoods, we found no errors at mask sizes ranging from $L = 2.3$ to 6.9 m; thus, any mask size would be appropriate for this species. The LM method only worked well for Japanese black pine, with large errors (>40%) for all other species. Omission errors were the largest proportion of the errors in this method. In the CS method, we observed small errors for Japanese cedar and dawn redwood, but large errors (20%) for the other species. In addition, commission errors were greatest for some of the species and omission errors were greatest for other species. This shows that the performance of the CS method depends on the tree species. The mean values of omission, commission, and total errors for all species combined were 8.1%, 1.6%, and 9.7%, respectively, for CE filtering versus 43.5%, 10.1%, and 53.6% for the LM method and 10.9%, 10.1%, and 21.0% for the CS method.

4 Discussion

Appropriate selection of mask size is important in CE filtering because the mask size determines the sensitivity of tree crown detection. CE filtering with a small mask size allows detection of both large and small tree crowns. However, adopting a too-small mask size can lead to incorrect identification of a region around local maxima that are caused by unevenness of the canopy surface as tree crowns, resulting in commission errors. This explains the results in Fig. 5, where many commission errors were observed at the smallest mask sizes. Thus, commission errors should decrease as the mask size increases, and Fig. 5 supports this hypothesis; few commission errors were observed at a mask size of $L = 1.9$ m or more. However, small tree crowns are less likely to be detected as the mask size increases because these crowns may be regarded as part of a larger tree's crown, particularly when a small tree is close to a large tree. This explains the gradual increase in omission errors as the mask size increases beyond $L = 1.9$ m in Fig. 5. As a result of these two offsetting changes, the total error was minimized at a mask size of $L = 1.9$ m, which corresponded to the smallest canopy diameter of Japanese cedar estimated from the DCHM for site 1. The most appropriate mask sizes for the other species were also close to the smallest canopy diameters of each species. Thus, the smallest canopy diameter of each species estimated from the DCHM can be used as a criterion to select an appropriate mask size in CE filtering.

Our comparison of the three detection methods revealed that CE filtering offered the most accurate results for most of the species. The LM method worked poorly for most of the tree

species at all strengths of Gaussian smoothing. The variable window size, based on the semivariance range of each of pixels, was not effective for the canopy structures at sites 1 and 2. Also in a previous study,[24] this method did not work well in canopies of mixed species with structural variability. Those results show that it is difficult in this method to change the mask (window) size appropriately to account for variations in canopy structure. In the CS method, all local-maxima were identified as tree apex candidates. These points included both true tree apexes and local maxima that resulted from canopy unevenness. Thus, commission errors occurred when the canopy was uneven. Fortunately, these errors can be reduced by increasing the strength of smoothing (Fig. 6). Consequently, the number of errors strongly depended on the strength of the smoothing. The relationship between the number of errors and smoothing strength has also been investigated in a previous study conducted in a natural forest reserve dominated by Norway spruce [*Picea abies* (L.) Karst.].[25] In this study, similar results to the present study were reported, i.e., commission errors in the CS method decreased drastically as smoothing (Gaussian) strength increased. Those results show that the selection of an appropriate smoothing strength is important for improving the accuracy of this method.

Currently, in the CS method, there is no clear criterion that can be used to select the most suitable smoothing strength for each tree species. This is a disadvantage of the CS method because the results will vary for different coniferous species. In contrast, the CE filtering method excludes a local maximum that is not a tree apex when the frame of the mask touches points around that local maximum. This is affected by whether the mask size was appropriately selected rather than by the smoothing strength that is applied; as a result, the error frequency in CE filtering is insensitive to the smoothing strength (Fig. 6). In practice, a moderate level of smoothing is enough to obtain accurate results in CE filtering. Although the smoothing strength is not important in CE filtering, it is still necessary to select a mask size that is appropriate for each coniferous species. However, a criterion to select the mask size appropriate for each coniferous species has been demonstrated above. Thus, CE filtering has advantages over the other two methods for a range of coniferous species.

5 Conclusions

Our results demonstrate that tree apexes can be detected accurately using DCHMs for coniferous trees derived using airborne LIDAR data combined with the newly developed CE filtering method. In this method, a square mask is used, with a frame at the edges. The mask overlaps the DCHM image, and pixels corresponding to tree crowns are extracted from the image by checking whether any pixels touch the mask's frame. Each tree apex is identified by choosing the pixel with the maximum height from the group of pixels that comprise a tree crown. We tested this method using a range of mask sizes in stands of Japanese cedar and of several coniferous species, and confirmed that the method provides accurate results when the most appropriate mask size is chosen. Our results also revealed that the most appropriate mask size was comparable to the smallest canopy diameter for a species (estimated manually and interactively from the DCHM). The smoothing strength chosen for the DCHM had little effect on the accuracy of the CE filtering.

Our comparison of the three methods revealed that the other two methods of tree apex detection were less accurate than CE filtering for most of the tree species that we studied. Our results suggest that CE filtering would be suitable for other coniferous canopies, but this should be confirmed by studying more coniferous species at more study sites. Although canopy surface was well reproduced in the DCHM images at the survey configuration of this study, fidelity of canopy surface reproduction could vary depending on LIDAR measurement conditions such as scan angle or laser footprint spacing on canopy surface. This may affect accuracy of tree apex detection by CE filtering. Therefore the robustness of CE filtering at different measurement conditions should be also investigated by additional works. Moreover, it is helpful to know tree species a priori for better performance of CE filtering, so combination between CE filtering and other remote sensing techniques that enable tree species classification (e.g., multi or hyper spectral imaging, etc.) is an interesting research subject. The present method is applicable only for confers and is difficult to be applied to nonconiferous canopy (e.g., deciduous canopy).

To cope with the limitation, it is required to modify the present method, extracting and utilizing features of shapes of nonconiferous canopy.

References

1. K. Omasa et al., "Accurate estimation of forest carbon stocks by 3-D remote sensing of individual trees," *Environ. Sci. Tech.* **37**, 1198–1201 (2003), http://dx.doi.org/10.1021/es0259887.
2. Z. J. Bortolot and R. H. Wynne, "Estimating forest biomass using small footprint LIDAR data: an individual tree-based approach that incorporates training data," *ISPRS J. Photogramm. Rem. Sens.* **59**, 342–360 (2005), http://dx.doi.org/10.1016/j.isprsjprs.2005.07.001.
3. K. Lim et al., "LIDAR remote sensing of biophysical properties of tolerant northern hardwood forests," *Can. J. Rem. Sens.* **29**, 658–678 (2003), http://dx.doi.org/10.5589/m03-025.
4. Y. Nakai, F. Hosoi, and K. Omasa, "Estimating carbon stocks of coniferous woody canopy trees using airborne LIDAR and passive optical sensor," in *Proc. ISPRS Laser scanning 2009*, XXXVIII, Part 3/W8 congress, ISPRS, Paris, pp. 289–292 (2009).
5. G. Patenaude et al., "Quantifying forest above ground carbon content using LIDAR remote sensing," *Rem. Sens. Environ.* **93**, 368–380 (2004), http://dx.doi.org/10.1016/j.rse.2004.07.016.
6. E. Næsset, "Determination of mean tree height of forest stands using airborne laser scanner data," *ISPRS J. Photogramm. Rem. Sens.* **52**(2), 49–56 (1997), http://dx.doi.org/10.1016/S0924-2716(97)83000-6.
7. M. Nilsson, "Estimation of tree heights and stand volume using an airborne LIDAR system," *Rem. Sens. Environ.* **56**, 1–7 (1996), http://dx.doi.org/10.1016/0034-4257(95)00224-3.
8. J. B. Drake et al., "Estimation of tropical forest structural characteristics using large-footprint LIDAR," *Rem. Sens. Environ.* **79**, 305–319 (2002), http://dx.doi.org/10.1016/S0034-4257(01)00281-4.
9. D. J. Harding et al., "Laser altimeter canopy height profiles: methods and validation for closed-canopy, broadleaf forests," *Rem. Sens. Environ.* **76**, 283–297 (2001), http://dx.doi.org/10.1016/S0034-4257(00)00210-8.
10. M. A. Hofton et al., "Validation of vegetation canopy LIDAR sub-canopy topography measurements for a dense tropical forest," *J. Geodyn.* **34**, 491–502 (2002), http://dx.doi.org/10.1016/S0264-3707(02)00046-7.
11. M. A. Lefsky et al., "LIDAR remote sensing for ecosystem studies," *BioSci.* **52**, 19–30 (2002).
12. J. E. Means et al., "Use of large-footprint scanning airborne LIDAR to estimate forest stand characteristics in the Western Cascades of Oregon," *Rem. Sens. Environ.* **67**, 298–308 (1999), http://dx.doi.org/10.1016/S0034-4257(98)00091-1.
13. K. Omasa et al., "3-D remote sensing of woody canopy heights using a scanning helicopter-borne LIDAR system with high spatial resolution," *J. Rem. Sens. Soc. Jpn.* **20**, 394–406 (2000), http://dx.doi.org/10.1037/a0020824.
14. K. Omasa et al., "Three-dimensional modelling of an urban park and trees by combined airborne and portable on-ground scanning LIDAR remote sensing," *Environ. Model. Assess.* **13**, 473–481 (2008), doi: http://dx.doi.org/10.1007/s10666-007-9115-5.
15. T. Brandtberg et al., "Detection and analysis of individual leaf-off tree crowns in small footprint, high sampling density LIDAR data from the eastern deciduous forest in North America," *Rem. Sens. Environ.* **85**, 290–303 (2003), http://dx.doi.org/10.1016/S0034-4257(03)00008-7.
16. J. Holmgren and Å. Persson, "Identifying species of individual trees using airborne laser scanner," *Rem. Sens. Environ.* **90**, 415–423 (2004), http://dx.doi.org/10.1016/S0034-4257(03)00140-8.
17. F. Hosoi, Y. Nakai, and K. Omasa, "Estimation and error analysis of wood canopy leaf area density profiles using 3-D airborne and ground-based scanning LIDAR remote-sensing

techniques," *IEEE Trans. Geosci. Rem. Sens.* **48**, 2215–2222 (2010), http://dx.doi.org/10.1109/TGRS.2009.2038372.
18. J. Hyyppä et al., "A segmentation-based method to retrieve stem volume estimates from 3-D tree height models produced by laser scanners," *IEEE Trans. Geosci. Rem. Sens.* **39**, 969–975 (2001), http://dx.doi.org/10.1109/36.921414.
19. E. Næsset et al., "Laser scanning of forest resources: the Nordic experience," *Scand. J. For. Res.* **19**, 482–499 (2004), http://dx.doi.org/10.1080/02827580410019553.
20. H. O. Ørka, E. Næsset, and O. M. Bollandsås, "Classifying species of individual trees by intensity and structure features derived from airborne laser scanner data," *Rem. Sens. Environ.* **113**, 1163–1174 (2009), http://dx.doi.org/10.1016/j.rse.2009.02.002.
21. X. W. Yu et al., "Automatic detection of harvested trees and determination of forest growth using airborne laser scanning," *Rem. Sens. Environ.* **90**, 451–462 (2004), http://dx.doi.org/10.1016/j.rse.2004.02.001.
22. Å. Persson, J. Holmgren, and U. Söderman, "Detecting and measuring individual trees using an airborne laser scanner," *Photogramm. Eng. Rem. Sens.* **68**, 925–932 (2002).
23. S. C. Popescu and R. H. Wynne, "Seeing the trees in the forest: using LIDAR and multispectral data fusion with local filtering and variable window size for estimating tree height," *Photogramm. Eng. Rem. Sens.* **70**, 589–604 (2004).
24. H. Huang et al., "Improving measurement of forest structural parameters by co-registering of high resolution aerial imagery and low density LIDAR data," *Sensors* **9**, 1541–1558 (2009), http://dx.doi.org/10.3390/s90301541.
25. S. Solberg, E. Næsset, and O. M. Bollandsas, "Single tree segmentation using airborne laser scanner data in a structurally heterogeneous spruce forest," *Photogramm. Eng. Rem. Sens.* **72**, 1369–1378 (2006).
26. M. Wulder, K. O. Niemann, and D. G. Goodenough, "Local maximum filtering for the extraction of tree locations and basal area from high spatial resolution imagery," *Rem. Sens. Environ.* **73**, 103–114 (2000), http://dx.doi.org/10.1016/S0034-4257(00)00101-2.
27. M. Wulder, K. O. Niemann, and D. G. Goodenough, "Error reduction methods for local maximum filtering of high spatial resolution imagery for locating trees," *Can. J. Rem. Sens.* **28**, 621–628 (2002).

Fumiki Hosoi received his ME and PhD degrees from the University of Tokyo, Tokyo, Japan, in 1995 and 2008, respectively. In 1995, he joined the Opto-Technology Laboratory, Furukawa Electric Company, Ltd., Ichihara, Chiba, Japan. He is currently with the Graduate School of Agricultural and Life Sciences, University of Tokyo.

Hiroaki Matsugami received an ME degree in 2006 from the University of Tokyo, Tokyo, Japan, in the Department of Agricultural and Life Sciences.

Kenichi Watanuki received an ME degree in 2002 from the University of Tokyo, Tokyo, Japan, Department of Agricultural and Life Sciences.

Yo Shimizu is currently with the Graduate School of Agricultural and Life Sciences, University of Tokyo.

Kenji Omasa received his ME degree from Ehime University, Ehime, Japan, in 1975 and his PhD degree in engineering from the University of Tokyo, Tokyo, Japan. He is currently a professor with the Department of Agricultural and Life Sciences, University of Tokyo. His research interests include imaging at scales ranging from the cellular level to the whole-plant level, remote sensing, modeling of ecosystems, analysis of the effects of global change on ecosystems, and information engineering for biological and environmental systems.